



ELSEVIER

Physica D ■ (■■■■) ■■■-■■■

www.elsevier.com/locate/physd

Acceleration of heavy and light particles in turbulence: Comparison between experiments and direct numerical simulations

R. Volk^{a,*}, E. Calzavarini^b, G. Verhille^a, D. Lohse^b, N. Mordant^c, J.-F. Pinton^a, F. Toschi^{d,e}

^a *Laboratoire de Physique, de l'École normale supérieure de Lyon, CNRS UMR5672, 46 Allée d'Italie, 69007 Lyon, France*

^b *Faculty of Science, J.M. Burgers Centre for Fluid Dynamics, and Impact-Institute, University of Twente, 7500 AE Enschede, The Netherlands*

^c *Laboratoire de Physique, Statistique de l'École normale supérieure de Paris, CNRS UMR8550, 24 rue Lhomond, 75005 Paris, France*

^d *Istituto per le Applicazioni del Calcolo CNR, Viale del Policlinico 137, 00161 Roma, Italy*

^e *INFN, Sezione di Ferrara, Via G. Saragat 1, I-44100 Ferrara, Italy*

Abstract

We compare experimental data and numerical simulations for the dynamics of inertial particles with finite density in turbulence. In the experiment, bubbles and solid particles are optically tracked in a turbulent flow of water using an Extended Laser Doppler Velocimetry technique. The probability density functions (PDF) of particle accelerations and their auto-correlation in time are computed. Numerical results are obtained from a direct numerical simulation in which a suspension of passive pointwise particles is tracked, with the same finite density and the same response time as in the experiment. We observe a good agreement for both the variance of acceleration and the autocorrelation time scale of the dynamics; small discrepancies on the shape of the acceleration PDF are observed. We discuss the effects induced by the finite size of the particles, not taken into account in the present numerical simulations.

© 2008 Elsevier B.V. All rights reserved.

PACS: 47.27.Jv; 47.27.Gs; 02.50.-r

Keywords: Inertial particles; Lagrangian acceleration; Lagrangian turbulence

1. Introduction

Understanding the transport of inertial particles with finite density, such as sediments, neutrally buoyant particles or bubbles in turbulent flows of water is of practical interest for both industrial engineering or environmental problems. In a turbulent flow, the mismatch in density between the particles and the fluid causes light particles to be trapped in high vortical regions while heavy particles are ejected from vortex cores and concentrate in high strain regions [1]. As particles with different buoyancy tend to concentrate in different regions of the flow, they are expected to exhibit different dynamic behaviours. In recent years, significant progress has been made in the limit of infinitely heavy, pointwise particles [2,3], and numerical simulations have received

experimental support [4,5]. In case of infinitely light particles (*bubbles*): the result of the numerical simulations on particle distributions and on fluid velocity spectra [6–8] agree in various aspects with experimental findings [9–12] although direct comparison between experiments and numerical simulations for the acceleration PDF and correlation of the particles has not been investigated in the past.

Indeed, in spite of the growing resolution of Direct Numerical Simulations (DNS) of the Navier-Stokes equations at high Reynolds numbers, it remains a challenge to resolve the motion of realistic inertial particles: some degree of modelization is necessary. The equation of motion of finite size, finite density particles moving in a turbulent flow, is not precisely known, and a comparison with experimental data can help in refining the models and extending their range of validity.

Several experimental techniques have been developed for measuring the velocity of particles along their trajectories. The optical tracking method developed in the Cornell group

* Corresponding author. Tel.: +33 472728472; fax: +33 472728080.

E-mail address: romain.volk@ens-lyon.fr (R. Volk).

has revealed that fluid particles experience extremely intense accelerations [13], while individual particles have been tracked for time durations of the order of the flow integral time scale using an acoustic technique [14]. Because of the very fast decrease of the acoustic scattering cross-section with the scatterer's size, this method is limited to particles with diameter of the order of the wavelength, *i.e.* inertial range sizes [15, 23]. The principle of the acoustic technique is completely analogous to laser Doppler velocimetry (LDV), provided that expanded light beams are used (an arrangement we call E-LDV hereafter). The advantage of E-LDV, compared to acoustics, is that the much smaller wavelength of light allows a better resolution in space and also the use of smaller tracer particles. The principle of the measurement technique is reported in [16], where its performance has been compared and validated against silicon-strip tracking [13,17] of neutrally buoyant Lagrangian tracers. We focus here on the dynamics of inertial particles *i.e.* particles whose density differ from that of the fluid. We report the first comparison between experimental measurements of acceleration of particles having a relative density in the range 10^{-3} (air bubbles) to 1.4 (PMMA) in the same highly turbulent flow, and numerical results obtained by tracking pointwise particles with finite density in a direct numerical simulation of isotropic homogeneous turbulence [18,19].

Numerical simulations are performed by means of standard pseudo-spectral methods, where particular care has been used in keeping a good resolution at the dissipative scales. The numerical code for integrating the evolution of the Eulerian field and the Lagrangian tracing of particles is the same as described in [7,8,25]. A thorough validation of the numerical approach, included the Lagrangian evolution of the tracers has recently been performed against experimental measurements [26]. The numerical integration of tracers has, with respect to experiments, the clear advantage of a uniform, well controlled geometry and very large statistics; on the opposite, the resolution can be limited to small Reynolds numbers. For what concerns the treatment of realistic particles, *i.e.* particles with a density mismatch and a “finite” size, the best modelization to use is not clear and one of the main goals of this manuscript is indeed to compare state-of-the-art Lagrangian data against numerical results from a current modelization.

2. Experimental setup and results

The Laser Doppler technique is based on the same principle as the ultrasound Doppler method which has good tracking performance of individual Lagrangian tracers [14,23]. In order to access dissipative scales, and in particular for acceleration measurements, we adapt the technique from ultrasound to laser light: the gain is of a factor 1000 in wavelength so that one expects to detect micron-sized particles. For a Lagrangian measurement, one has to be able to follow the particle motion to get information about its dynamics in time. For this, wide Laser beams are needed to illuminate the particle on a significant fraction of its path. The optical setup is an extension of the well known laser Doppler velocimetry technique; Fig. 1. A Laser beam is split into two beams; each is then expanded by

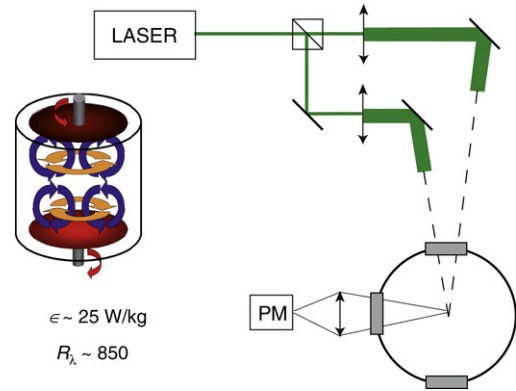


Fig. 1. Experimental setup. (Top left): schematics of the von Kármán flow in water – side view. (Top right): principle of the Laser-Doppler Velocimetry using wide beams (ELDV) – top view of the experiment. PM: location of the photomultiplier which detects scattering light modulation as a particle crosses the interference pattern created at the intersection of the laser beams.

a telescope so that their diameter is about 5 mm. Then the two beams intersect in the flow where they create an array of interference fringes. As a particle crosses the fringes, the scattered light is modulated at a frequency directly proportional to the component of the velocity perpendicular to the fringes. It yields a measurement of one component of the particle velocity. In practice, we use a CW YAG laser of wave length 532 nm with 1.2 W maximum output power. In order to get the sign of the velocity we use acousto-optic modulators (AOM) to shift the frequency of the beams so that the fringes are actually travelling at a constant speed. The angle of the two beams is tuned to impose a 60 microns inter-fringe so that the frequency shift between the beams (100 kHz) corresponds to 6 m/s. As the beams are not focused, the inter-fringe remains constant across the measurement volume whose size is about $5 \times 5 \times 10 \text{ mm}^3$. It is imaged on a photomultiplier whose output is recorded using a National Instrument PXI-NI5621 digitizer at rate 1 MHz.

The flow is of the Von Kármán kind as in several previous experiments using acoustics [14] or optical techniques [13]. Water fills a cylindrical container of internal diameter 15 cm, length 20 cm. It is driven by two disks of diameter 10 cm, fitted with blades in order to increase steering. The rotation rate is fixed at values up to 10 Hz. For the measurements reported here, the Taylor-based Reynolds number reaches up to 850 at a maximum dissipation rate ϵ equal to 25 W/kg. We study three types of particles: neutrally buoyant polystyrene particles with size 31 microns and density 1.06, PMMA particles with size 43 microns and density 1.4 and air bubbles with a size of about 150 microns. The mean size of the bubbles, measured optically by imaging the measurement volume on a CCD, is imposed by the balance between the interfacial surface tension σ and the turbulent fluctuations of pressure. This fragmentation process is known to lead to a well defined and stationary size distribution [20] with a typical diameter $D \propto (\sigma/\rho_f)^{3/5} \epsilon^{-2/5}$, ρ_f being the density of the fluid.

The signal processing step is crucial as both time and frequency – (*i.e.* velocity) – resolutions rely on its performance. Frequency demodulation is achieved using the same algorithm as in the acoustic Doppler technique. It is a approximated

Table 1

(top) Parameters of the particles in the von Kármán flow at $R_\lambda = 850$ ($\eta = (\nu^3/\epsilon)^{1/4} = 17 \mu\text{m}$ and $\tau_\eta = \sqrt{\nu/\epsilon} = 0.26 \cdot 10^{-3} \text{ s}$)

Experiment					
Particle	Radius a	$\beta = \frac{3\rho_f}{\rho_f+2\rho_p}$	$St = \frac{\tau_p}{\tau_\eta}$	a_0	$a_0/a_{0,T}$
Tracers	15.5 μm	0.96	0.24	6.4 ± 1	1
Neutral	125 μm	0.96	16	2.2 ± 1	0.34
Heavy	20.5 μm	0.79	0.58	4.3 ± 1	0.67
Bubble	75 μm	2.99	1.85	26 ± 5	4.06
Numerics					
Particle	Radius a	$\beta = \frac{3\rho_f}{\rho_f+2\rho_p}$	$St = \frac{\tau_p}{\tau_\eta}$	a_0	$a_0/a_{0,T}$
Tracers	–	1	0.31	2.85 ± 0.07	1
Neutral	–	1	4.1	2.94 ± 0.07	1.03
Heavy	–	0.75	1.03	2.63 ± 0.12	0.92
Bubble	–	3	1.64	25.9 ± 0.46	9.08

ρ_p and ρ_f are the densities of the particles and fluid, and $\tau_p = a^2/(3\beta\nu)$ is the Stokes response time of the particles. The Taylor-based turbulent Reynolds number is computed as $R_\lambda = \sqrt{15u_{\text{rms}}^4/\epsilon}$ measuring the one-component root-mean-square velocity, u_{rms} , with the E-LDV system and ϵ by monitoring the power consumption of the motors. The nondimensional constant a_0 is derived from the Heisenberg–Yaglom relationship. The last column compares the value for the inertial particle to the one obtained for the Lagrangian tracer (which is denoted by the subscript T). (bottom) Same as above: parameters of the particles tracked in the DNS of homogeneous isotropic turbulence at $R_\lambda = 180$. Out of the numerically analysed 64 parameter combinations (β , St), we have picked those which were close to the experimental values for (β , St).

maximum likelihood method coupled with a Kalman filter [21]: a parametric estimator assumes that the signal is made of a modulated complex exponential and Gaussian noise. The amplitude of the recorded signal and the modulation frequencies are assumed to be slowly evolving compared to the duration of the time window used to estimate the instantaneous frequency. Here the time window is about 30 μs long and sets the time resolution of the algorithm. Outputs of the algorithm are the instantaneous frequency, the amplitude of the modulation and a confidence estimate which is used to eliminate unreliable detections. Afterwards, the acceleration of the particle is computed by differentiation of the velocity output. Note that measurements are performed only when a particle moves within the (limited) measurement volume so that after processing, the data consists in a collection of sequences with variable lengths. For all the measurements, the acceleration variance is computed using the same procedure as in [17]: it is obtained for several widths of the smoothing kernel used in the differentiation of the velocity signal and then interpolated to zero filter width.

For small neutrally buoyant particles, *i.e.* Lagrangian tracers, our data is in excellent agreement with the high-speed imaging measurements performed by the Cornell group [13,16,17]. When the variance of the acceleration is normalized by the Heisenberg–Yaglom scaling: $\langle a^2 \rangle = a_0 \epsilon^{3/2} \nu^{-1/2}$ (ϵ being the energy dissipation rate per unit mass and $\nu = 1.3 \cdot 10^{-6} \text{ m}^2 \text{ s}^{-1}$ the kinematic viscosity of the fluid), both experiments yields the same values for the nondimensional constant a_0 ($a_0 = 6.4 \pm 1$ at $R_\lambda = 850$ for the E-LDV compared to 6.2 ± 0.4 for the Cornell data at $R_\lambda = 690$).

We have applied our technique to compare the dynamics of Lagrangian tracers to the one of heavier or lighter particles (see Table 1 for numbers). We first compute the velocity root-mean-square value u_{rms} for the three cases: the values are $\{1.1, 1.2, 1.0\} \pm 0.1 \text{ m}\cdot\text{s}^{-1}$ at $R_\lambda = 850$ for the tracers,

heavy (PMMA spheres), and light particles (bubbles). Within error bars, the large scale dynamics seems to be unaffected by changes in the particle inertia. The acceleration distribution and autocorrelation in the three cases are shown respectively in Fig. 2 (top) and Fig. 3 (top). The acceleration PDFs are quite similar for moderate acceleration values (below about $10 a_{\text{rms}}$), as also observed in low Reynolds number numerical simulations [22]. However, the probability of very large accelerations seems to be reduced in the case of inertial particles as compared to Lagrangian tracers. The normalized acceleration variance a_0 varies very significantly: it is reduced to 4.3 ± 1 for heavier particles while it is increased to 26 ± 5 for bubbles. The correlation functions also show significant changes with inertia: the characteristic time of decay is longer for heavy particles and shorter for bubbles compared to tracers. We measure $\tau_{\text{corr}}/\tau_\eta = \{0.5, 0.9, 0.25\}$ respectively for tracers, heavy and light particles, with the correlation time defined as the half-width at mid-amplitude of the correlation function. We thus observe important changes in the dynamics, even if the distribution of acceleration weakly changes with inertia.

Note that in our setup the Kolmogorov length is about $\eta = 17 \mu\text{m}$ at $R_\lambda = 850$, so that the bubble size is about 10η and therefore may not be considered as a point particle. Thus, one may wonder if the bubble dynamics is not altered by spatial filtering as recently demonstrated for particles with diameters in the inertia range [23]. To check, we have compared the dynamics of large neutrally buoyant particles with diameter $250 \mu\text{m}$ to the one of Lagrangian tracers. The results is shown in Fig. 2 together with the other particles: the effect of the particle size on the PDF is found to be weak as the curve nicely superimposes with the ones for inertial particles. However, the size effect is clear when comparing either the coefficient a_0 (reduced to 2.2), or the autocorrelation functions. One observes that the correlation time of the large particles is twice that

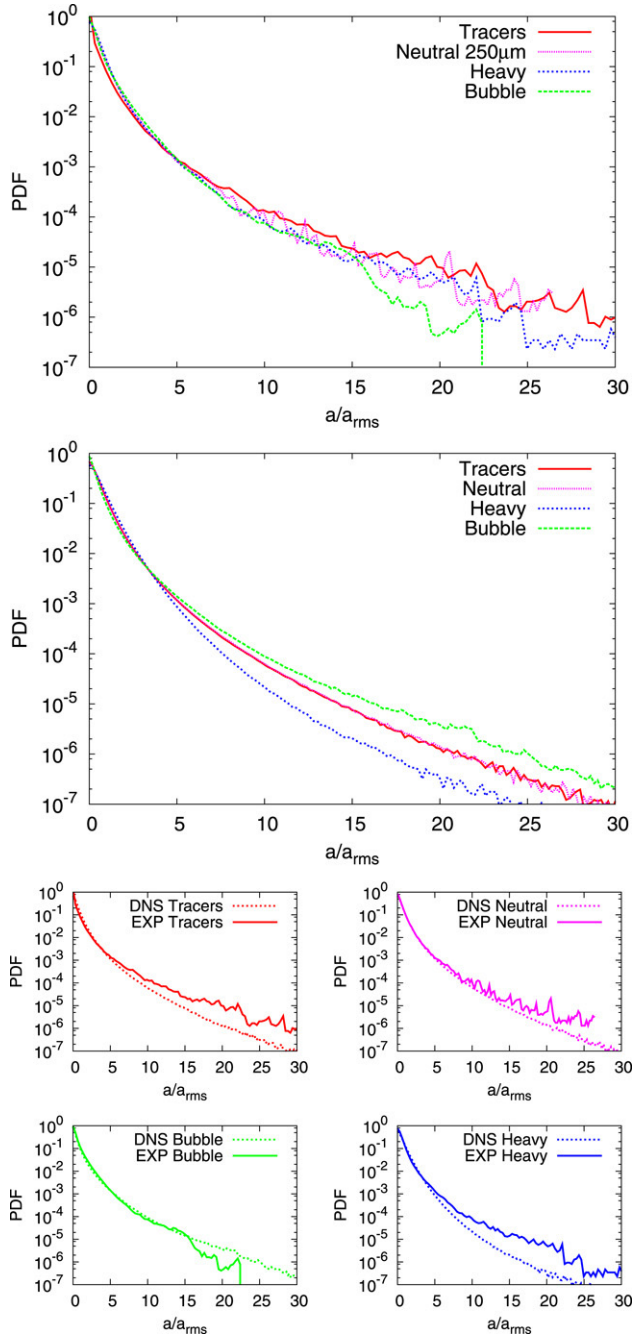


Fig. 2. Probability distribution function of accelerations, normalized to the variance of the data sets. (top) Data from experiment at $R_\lambda = 850$. (middle) DNS of homogeneous isotropic turbulence at $R_\lambda = 180$. (bottom) Comparison of experimental measurements and DNS results.

for the tracers. We conclude that the bubbles size may have a leading effect on the acceleration variance, and that the value of a_0 reported here probably underestimates the one that would be measured for smaller bubbles (with diameters closer to the Kolmogorov scale).

3. Comparison with numerical simulations

We compare the experimental data with the results from a direct numerical simulation [18,19] where a passive suspension

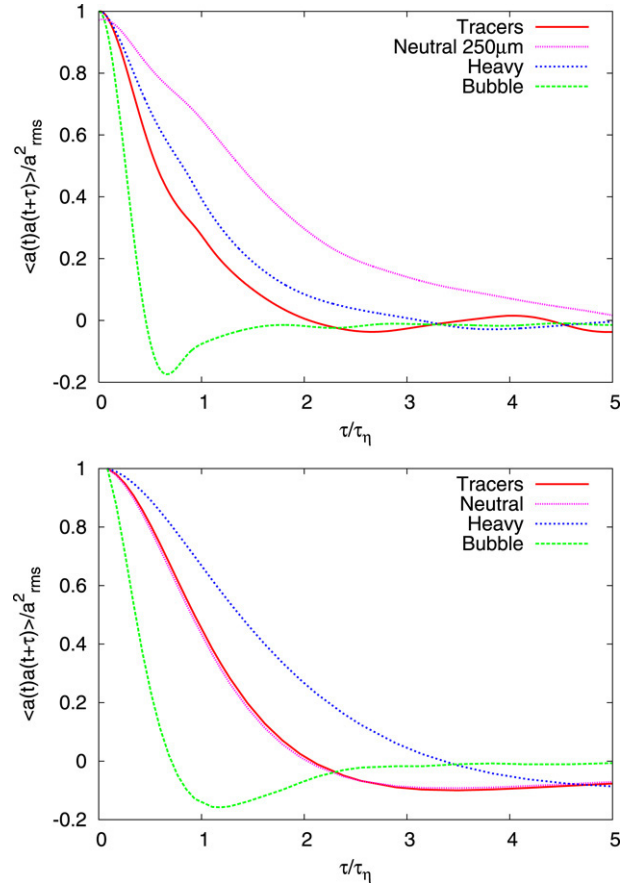


Fig. 3. Autocorrelation coefficients of the accelerations: (top) Data from experiments at $R_\lambda = 850$. (bottom) Data from DNS of homogeneous isotropic turbulence at $R_\lambda = 180$. For the (β, St) values we refer to Table 1.

of pointwise particles with finite density are tracked in a homogeneous isotropic turbulent flow. The dynamics of the particles is computed in the most simplified form of the equation of motion, *i.e.* assuming that the particles are spherical, nondeformable, smaller than the Kolmogorov length scale of the flow, and that their Reynolds number is small [24]. When we retain only the Stokes drag force and the added mass effect, the equation of motion then reads

$$\frac{d\mathbf{v}_p}{dt} = \beta \frac{D\mathbf{u}}{Dt} + \frac{1}{\tau_p} (\mathbf{u} - \mathbf{v}_p), \quad (1)$$

where $\mathbf{v}_p = \dot{\mathbf{x}}(t)$ is the particle velocity, $\mathbf{u}(\mathbf{x}(t), t)$ the velocity of the fluid at the location of the particle described by the Navier–Stokes equation, while $\beta = 3\rho_f/(\rho_f + 2\rho_p)$ accounts for the added mass effect and $\tau_p = a^2/(3\beta\nu)$ is the Stokes response time for a particle of radius a . When made dimensionless by the Kolmogorov dissipative scales $(\tau_\eta, \eta, u_\eta)$ Eq. (1) reads

$$\mathbf{a} \equiv \frac{d\mathbf{v}_p}{dt} = \beta \frac{D\mathbf{u}}{Dt} + \frac{1}{St} (\mathbf{u} - \mathbf{v}_p), \quad (2)$$

with the particle acceleration \mathbf{a} now expressed in the Heisenberg–Yaglom units. Thus, at a given Reynolds number, the particles dynamics only depends on the values of the two dimensionless parameters β and $St = \tau_p/\tau_\eta$. This is generally

different from the case of infinite inertia of the particles ($\beta = 0$) and finite response time τ_p , which has been formerly addressed in several numerical and theoretical studies [2], and for which instead only the Stokes number St matters. It is also different from the pure bubble case ($\beta = 3$) for which the particle indeed has no inertia but only added mass [6–8]. We performed numerical simulation at $Re_\lambda = 180$ (grid resolution 512^3), in which many particles, characterized by different pairs, (β, St) (specifically 64 different sets of $O(10^5)$ particles) were numerically integrated by means of Eq. (1). Particles do not have feedback on the flow field.

In order to compare the numerical results with the experimental data, three types of particles (tracers, heavy and bubbles) with different inertia and Stokes number have been studied. The values for both β and St have been chosen close to the ones of the particles used for the E-LDV (see Table 1). The evolution of the normalized acceleration variance shows the same trend in experiments and numerics: a_0 is reduced from the tracer value 2.85 to 2.63 for heavier particles and increased to 26 for bubbles (Table 1). This seems to be a robust trend in the DNS. To emphasize this, in Fig. 4 we show the behaviour of $\sqrt{a_0}$, i.e. the root-mean-square value of the particle acceleration normalized by the Heisenberg–Yaglom scaling, in a wide range of the (β, St) parameter space from a less turbulent DNS ($Re_\lambda = 75$) which has a very large number of (β, St) pairs. Results from the $Re_\lambda = 180$, not shown here, are qualitatively similar. Note again that no significant Reynolds number dependence of the probability distribution was found in Ref. [16].

The acceleration distribution behavior and its comparison with the experiment is reported in Fig. 2. In the numerics we observe that the probability of very large accelerations is reduced for the heavier particles as compared with tracers, while it is increased for the bubbles. This feature, seems not to be present in the experimental results. Furthermore, we notice that for the three types of particles, the acceleration PDFs, rescaled by the *rms* acceleration, is close to the experiments. Experimental ones have always longer tails, reflecting the more intermittent nature of the turbulent flow, which has a larger Reynolds number ($Re_{\lambda,EXP} = 850$ vs. $Re_{\lambda,DNS} = 180$). We also observe a qualitative agreement for the changes in the acceleration autocorrelation functions when changing inertia, Fig. 3. One measures $\tau_{corr}/\tau_\eta = \{0.95, 1.35, 0.25\}$ respectively for tracers, heavy and light particles. Just as observed for the experiments, the dynamics is faster for the bubbles while heavier particles decorrelate slower than fluid tracers. The Re_λ difference is more pronounced here than in the PDFs (see Ref. [16]) and prevent a more detailed comparison.

4. Discussion

While solving a simplified version for the equation of motion, the numerics reproduce qualitatively the effect of the particles' inertia on their dynamics. In particular, the dependence of the acceleration autocorrelation on the particle inertia is nicely reproduced, see Fig. 3. However, also some discrepancies become visible, though not yet completely

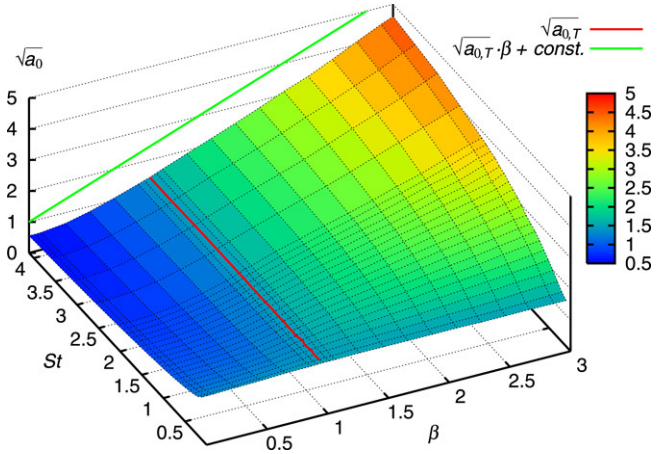


Fig. 4. Behaviour of the normalized root-mean-square acceleration $\sqrt{a_0} = ((a^2)\epsilon^{-3/2} \nu^{1/2})^{1/2}$ as a function of both St and β for a $Re_\lambda = 75$ DNS. Iso-contour for $\sqrt{a_{0,T}}$ (red) and the line $\sqrt{a_{0,T}} \cdot \beta + const.$ (green) are also reported. Note that a_0 does not depend on St for neutral ($\beta = 1$) particles. While it is always reduced/enhanced for heavy/light particles. For large particles ($St \simeq 4.1$) we find $\sqrt{a_0} \simeq \beta \sqrt{a_{0,T}}$. (For interpretation of the references to colour in this figure legend, the reader is referred to the web version of this article.)

conclusive, as a better resolution and statistics of both the experiments and the numerics would be important for firmer conclusions. Nevertheless, in this section we shall have a closer look at the differences and propose some explanations.

First of all, there is only qualitative agreement on the ratio $a_{0,H}/a_{0,T}$. It is larger for the experiment than for the numerics. Moreover, the tails of the numerical PDF of the bubble acceleration seem to be enhanced as compared to those for tracer acceleration. Vice versa, the tails of the numerical PDF of the particle acceleration seem to be reduced as compared to those for tracer acceleration.

What is the origin of the difference between the experiments and the numerics? First of all the Taylor–Reynolds numbers are different, but Ref. [16] suggests an at most weak dependence of the acceleration PDFs on the Reynolds number; a finding that is supported by a comparison of our numerical simulations at $Re_\lambda = 185$ and $Re_\lambda = 75$.

Next, in the numerical simulations we disregarded the lift and the gravitational force. While this presumably has little effect on heavy particles and tracer, it does modify the dynamics of the bubbles. In Refs. [7,8] we had shown by comparison of numerical simulations for point bubbles with and without lift, that without lift the bubble accumulation inside the vortices is more pronounced, i.e. bubbles without lift are more exposed to the small-scale fluctuations, which clearly will contribute to the pronounced tails of the numerically found acceleration PDF, see Fig. 3, bottom.

Next, also the two-way coupling of the particles (i.e., the back-reaction of the particles on the flow due to their buoyancy difference) has been neglected in the simulations of this paper. As e.g. shown in Refs. [7,8] for bubbles and in Ref. [27] for particles, it has an effect on the turbulent energy spectrum and thus also on the acceleration statistics. However, as in the present experiments the particle and bubble concentrations are

very low, the two-way coupling effect on the spectra should hardly be detectable.

The final difference between numerics and experiments we will discuss here – and presumably the most relevant one – is the finite size of the particles in the experiments as compared to the numerics which is based on effective forces on a point particle. Although the heavy particles are not large as compared to η , this clearly holds for the bubbles and the 250 μm diameter neutral particles. Indeed, Fig. 3 shows how the finite size of these particles smears out the acceleration autocorrelation, as compared to the tracer case. Also the ratio $a_{0,N}/a_{0,T}$ for large neutral particles is only 0.34, which demonstrates that the size of large particles has a large effect on their acceleration variance. This type of spatial filtering, which also lowers the PDF of large neutral particles in the experiment, is not related to a temporal filtering of the particle based on its response time. This is clearly visible in Fig. 2 (middle) where one can see that two neutral particles ($\beta = 1$) with different response times (different St or τ_p) have the same acceleration PDF, with same a_0 , and same autocorrelation function. Thus this size effect, which is not taken into account in the point-particle-based numerical simulations, presumably is responsible for both the relatively small value of $a_{0,B}/a_{0,T}$ measured for bubbles, and the change in the shape of the PDF.

To conclude, we have reported acceleration measurements of inertial particles using extended Laser Doppler velocimetry and have compared the experimental data to DNS simulations of the motion of pointwise particles with finite density. We have observed a qualitative agreement between experiments and numerics in the shape of the PDF and of the autocorrelation function. We have given arguments for the small discrepancies. An experimental study of the motion of bubbles with smaller sizes is needed for a better comparison with the numerical simulations. Also numerical simulations keeping into account the finite size of particles would presumably improve the agreement between experiments and numerical data and detailed comparisons as the one presented in this paper help to reveal the limitations of point-particle models. Obviously, going beyond point-particles is extremely challenging in numerical simulations. A first step in this direction has e.g. been taken by Prosperetti and coworkers with their *Physalis* method [28] which presently is extended towards turbulent flows [29].

Acknowledgements

RV, GV, NM and JFP are indebted to Artem Petrosian for his help in setting-up up the optics of the experiment, and to Mickael Bourgoin for many fruitful discussions. We are grateful to Massimo Cencini, who contributed to the numerical study. This work was partially funded by the Region Rhône-Alpes, under Emergence Contract No. 0501551301, and

by ANR contract #192604. We thank the CASPUR (Rome-ITALY), CINECA (Bologna-ITALY) and SARA (Amsterdam, The Netherlands) for computing time and technical support.

References

- [1] S. Sundaram, L.R. Collins, *J. Fluid Mech.* 379 (1999) 105.
- [2] J. Bec, M. Cencini, R. Hillerbrand, *Physica D* 226 (2007) 11; J. Bec, L. Biferale, M. Cencini, A. Lanotte, S. Musacchio, F. Toschi, *Phys. Rev. Lett.* 98 (2007) 084502.
- [3] M. Cencini, J. Bec, L. Biferale, G. Boffetta, A. Celani, A.S. Lanotte, S. Musacchio, F. Toschi, *J. Turb.* 7 (36) (2006) 1–17.
- [4] J.R. Fessler, J.D. Kulick, J.K. Eaton, *Phys. Fluids* 6 (1994) 3742–3749.
- [5] S. Ayyalasomayajula, A. Gylfason, L.R. Collins, E. Bodenschatz, Z. Warhaft, *Phys. Rev. Lett.* 97 (2006) 144507.
- [6] L. Wang, M.R. Maxey, *Appl. Sci. Res.* 51 (1993) 291–296.
- [7] I. Mazzitelli, D. Lohse, F. Toschi, *Phys. Fluids* 15 (2003) L5–L8.
- [8] I. Mazzitelli, D. Lohse, F. Toschi, *J. Fluid Mech.* 488 (2003) 283–313.
- [9] J.M. Rensen, S. Luther, D. Lohse, *J. Fluid Mech.* 538 (2005) 153–187.
- [10] T.H. van den Berg, S. Luther, I. Mazzitelli, J. Rensen, F. Toschi, D. Lohse, *J. Turb.* 7 (2006) 1–12.
- [11] T.H. van den Berg, S. Luther, D. Lohse, *Phys. Fluids* 18 (2006) 038103.
- [12] E. Calzavarini, T.H. van den Berg, S. Luther, F. Toschi, D. Lohse, Quantifying microbubble clustering in turbulent flow from single-point measurements, *Phys. Fluids* (2008) (in press). [arXiv:0607255](https://arxiv.org/abs/0607255).
- [13] G.A. Voth, A. La Porta, A.M. Crawford, J. Alexander, E. Bodenschatz, *J. Fluid Mech.* 469 (2002) 121.
- [14] N. Mordant, et al., *Phys. Rev. Lett.* 87 (21) (2001) 214501; N. Mordant, P. Metz, O. Michel, J.-F. Pinton, *Rev. Sci. Instr.* 76 (2005) 025105.
- [15] N. Mordant, E. L  v  que, J.-F. Pinton, *New J. Phys.* 6 (2004) 116.
- [16] R. Volk, N. Mordant, G. Verhille, J.-F. Pinton, Laser Doppler measurement of inertial particle and bubble accelerations in turbulence, *Eur. Phys. Lett.* (2008) (in press). [arXiv:0708.3350](https://arxiv.org/abs/0708.3350).
- [17] N. Mordant, A.M. Crawford, E. Bodenschatz, *Physica D* 193 (2004) 245; N. Mordant, A.M. Crawford, E. Bodenschatz, *Phys. Rev. Lett.* 94 (2004) 024501.
- [18] E. Calzavarini, M. Kerscher, D. Lohse, F. Toschi, Dimensionality and morphology of particle and bubble clusters in turbulent flow, *J. Fluid Mech.* (2007) (submitted for publication). [Arxiv:nlin.CD/0710.1705](https://arxiv.org/abs/nlin.CD/0710.1705).
- [19] E. Calzavarini, M. Cencini, D. Lohse, F. Toschi, Quantifying turbulence induced segregation of inertial particles, *Phys. Rev. Lett.* (2008) (submitted for publication). [arXiv:0802.0607](https://arxiv.org/abs/0802.0607).
- [20] C. Martinez-Baz  , J.-L. Montan  es, J.C. Lasheras, *J. Fluid Mech.* 401 (1999) 183–207.
- [21] N. Mordant, O. Michel, J.-F. Pinton, *J. Acoust. Soc. Am.* 112 (2002) 108–119.
- [22] I.M. Mazzitelli, D. Lohse, *New J. Phys.* 6 (2004) 203.
- [23] N. Qureshi, M. Bourgoin, C. Baudet, A. Cartellier, Y. Gagne, *Phys. Rev. Lett.* [arXiv:0706.3042](https://arxiv.org/abs/0706.3042) (in press).
- [24] M.R. Maxey, J. Riley, *Phys. Fluids* 26 (1983) 883.
- [25] L. Biferale, G. Boffetta, A. Celani, B. Devenish, A. Lanotte, F. Toschi, *Phys. Rev. Lett.* 93 (2004) 064502.
- [26] L. Biferale, E. Bodenschatz, M. Cencini, A.S. Lanotte, N.T. Ouellette, F. Toschi, H. Xu, [arXiv:0708.0311](https://arxiv.org/abs/0708.0311), 2007.
- [27] M. Boivin, O. Simonin, K.D. Squires, *J. Fluid Mech.* 375 (1998) 235–263.
- [28] Z. Zhang, A. Prosperetti, *J. Comput. Phys.* 210 (2005) 292–324; *J. Appl. Mech. - Transactions of the ASME* 70 (2003) 64–74.
- [29] A. Naso, A. Prosperetti, Proceedings of ICMF 2007, Leipzig (D) July 9–13, 2007.